ISBN: 978-3-95450-221-9 ISSN: 2226-0358 doi:10.18429/JACoW-ICALEPCS2021-WEPV003

THE DYNAMIC MODELING AND THE CONTROL ARCHITECTURE OF THE NEW HIGH-DYNAMIC DOUBLE-CRYSTAL MONOCHROMATOR (HD-DCM-Lite) FOR SIRIUS/LNLS

G. S. de Albuquerque*, A. V. Perna, J. L. Brito Neto, M. A. L. Moraes, M. S. Souza, M. Saveri Silva, R. R. Geraldes[1], LNLS, Campinas, Brazil
[1]also at the CST Group, Eindhoven University of Technology (TUe), Eindhoven, The Netherlands

Abstract

The High-Dynamic Double-Crystal Monochromator (HD-DCM) has been developed since 2015 at Sirius/LNLS with an innovative high-bandwidth mechatronic architecture to reach the unprecedented target of 10 nrad RMS (1 Hz - 2.5 kHz) in crystals parallelism also during energy flyscans. Now, for beamlines requiring a smaller energy range (3.1 keV to 43 keV, as compared to 2.3 keV to 72 keV), there is the opportunity to adapt the existing design towards the so-called HD-DCM-Lite. The control architecture of the HD-DCM is kept, reaching a 20 kHz control rate in NI's CompactRIO (cRIO). Yet, the smaller gap stroke between crystals allows for removing the long-stroke mechanism and reducing the main inertia by a factor 6, not only simplifying the dynamics of the system, but also enabling faster energy scans. With sinusoidal scans of hundreds of eV up to 20 Hz, this creates an unparalleled bridge between slow step-scan DCMs, and channel-cut quick-EXAFS monochromators. This work presents the dynamic error budgeting and scanning perspectives for the HD-DCM-Lite, including discussions on the feedback control via loop shaping, feedforward considerations, and leader-follower control strategies.

INTRODUCTION

After successfully designing, installing and commissioning the High-Dynamic Double-Crystal Monochromator (HD-DCM) [1] at the MANACÁ (crystallography) and the EMA (extreme conditions) beamlines, QUATI (quick absorption spectroscopy) and SAPUCAIA (small-angle-scattering) are two forthcoming Sirius beamlines demanding an HD-DCM at the Brazilian Synchrotron Light Laboratory (LNLS). Since these new beamlines require a smaller energy range (3.1 to 43 keV), the total gap stroke of the instrument can be significantly reduced from 9 mm to about 2.75 mm, such that an opportunity is created to adapt the existing design towards the so-called HD-DCM-Lite.

Removing the long-stroke module (see [1]) for the large gap adjustments allows not only for cost reduction and simplification in the assembly, but also for significant improvement in dynamics. By reducing the main inertia by a factor of 6, the HD-DCM-Lite is expected to deliver energy flyscans of hundreds of eV up to at least 4 to 40 times per second, while keeping fixed exit and the inter-crystal parallelism in the range of a few tens of nrad RMS (root mean square) for the 1 Hz - 2.5 kHz range. Thus, QUATI (superbend-based) may take full advantage of this capability in time-resolved analysis, whereas new science opportunities may be explored for SAPUCAIA. The new design focuses on extending the scanning capabilities while preserving positional accuracy, creating a solution between the current HD-DCM (limited in speed but with fixed-offset and already extremely stable) and fast channel-cut monochromators [2], which suffer from beam walk due to offset variation.

An overview of the mechanical design of the HD-DCM-Lite, with the CAD drawing of its in-vacuum mechanics and a simplified lumped-mass model, is given in Fig. 1. Two crystal sets, with Si(111) and Si(311) orientations for options in energy filtering bandwidth and range, are mounted side by side, being alternatively selected during operation. At the lower side, the so-called 1st Crystals (CR1) (6) are mounted to a common Metrology Frame (MF1) (5), which, in turn, is fixed to an Auxiliary Frame (AF1) (4), that is, finally, fixed to the Goniometer Frame (GOF) (3), which is driven by two rotary stages (ROT) (2) for controlling the angle of incidence of the incoming X-ray beam on the crystals for energy selection according to Bragg's law of diffraction.

At the upper side, the so-called 2nd Crystals (CR2) (7) are used to redirect the beam in the fixed-exit configuration that defines the operational principles of an X-ray DCM. They are mounted to a common metrology frame as well, which, in this case, is a Short-Stroke stage (SHS) (8) that is actively controlled with nanometer level with respect to the MF1 in 3 degrees of freedom (DOF). Indeed, the distance (gap) and parallelism between crystals — or, more precisely, between their metrology frames — can be adjusted via closed-loop control based on 3 voice-coil actuators and 3 laser interferometers. The reaction forces of these actuators act on a Balance-mass (BMS) (10) for dynamic filtering purposes, and both the SHS and the BMS are mounted via flexural folded leaf-springs to the Auxiliary frame 2 (AF2) (9), which is also fixed to the GOF.

The supports of the ROT are stiffly fixed to a vacuum flange, as part of the complete vacuum vessel (VES) (not shown), which, in turn, is stiffly fixed to a granite bench (GRA) (1) for alignment purposes and crystal set selection at the beamline, building the dynamic architecture of the system all the way up from experimental floor (GND).

With the previous experience from the HD-DCM as a high-end mechatronic system, here again a systematic approach based on precision engineering principles and predictive modeling has been adopted to maximize the efficiency in development time and costs, according to a "first-time-right"

* guilherme.sobral@lnls.br

ISBN: 978-3-95450-221-9 ISSN: 2226-0358 doi:10.18429/JACoW-ICALEPCS2021-WEPV003

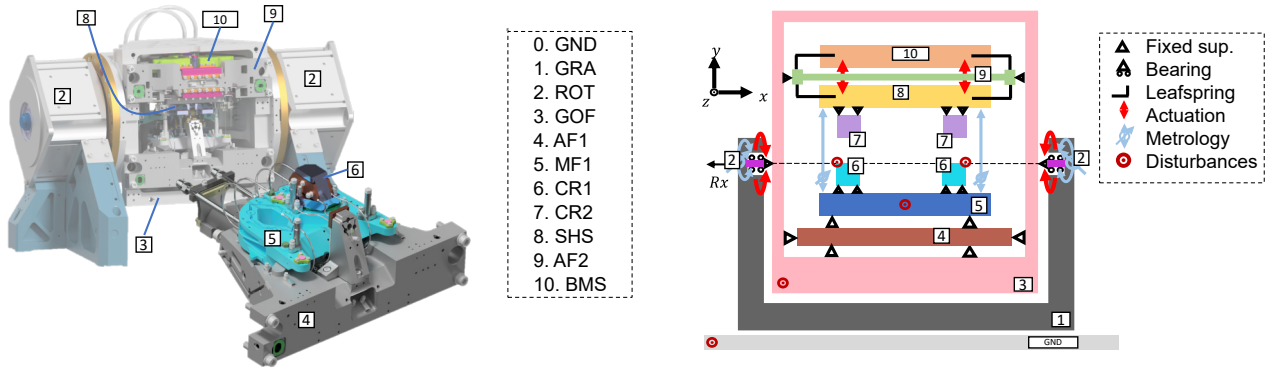

Figure 1: Left: HD-DCM-Lite in-vacuum main parts. Right: Lumped-mass model including actuators, sensors and disturbances, as used for dynamic error budgeting performance predictions.

philosophy. Using the Dynamic Error Budgeting (DEB) methodology [3, 4], the effects of system disturbances can be investigated as the mechatronic design of the machine is iteratively refined until compliance with specs.

Introductory aspects of the HD-DCM-Lite, such as the control effort, maximum displacement amplitude, speed budget, and thermal management, and the resulting time-resolved capabilities analysis were briefly introduced in [5]. Regarding its control architecture, it is expected to very closely follow the FPGA-based solution with NI's CompactRIO (cRIO) that has been developed for the HD-DCM, such that control rates up to 20 kHz should be possible for conformity with closed-loop bandwidths up to 250 Hz, or higher. The latest status in this topic, including integration aspects at Sirius beamlines can be found in [6].

Here, using a DEB toolbox that has been developed at LNLS during the HD-DCM project, the following sections discuss the mechatronic and disturbance models for the system, and present the high-performance predictions both in stand-still and scanning operation modes.

MECHATRONIC MODEL

As described below, the mechatronic model consists in a state-space representation composed of the electro-mechanical plant, including the mechanical dynamics, actuators and sensors, and the controllers.

Plant

The mechanical plant is developed according to the lumped-mass model shown in Fig. 1, with the mechanical system being derived in 6DOF via Dynamic Substructuring (DS) methods [7]. Firstly, inertia and geometrical parameters for each body are extracted from the CAD drawing in Autodesk® Inventor and exported to MATLAB® , where the whole customized toolbox has been implemented. Then, the links between lumps are defined as stiffness values, obtained either from simulated Structural Analysis with Ansys® Mechanical or from experimental data (see [3]). Next, the mechanical system is coupled via well-known DS transformations, written in state-space representation and put in modal basis, such that modal damping factors, based on experience or experimental results, can be individually applied to each mode shape. Finally, transformation matrices are computed to account for the geometry of the metrology points of sensors, and the action points of actuators and points subject mechanical disturbances.

Controllers

As the HD-DCM, the HD-DCM-Lite was designed in such way that the DOF of interest can be statically decoupled to transform the original multiple-input-multiple-output (MIMO) system in independent single-input-single-output (SISO) systems, which greatly simplifies the design of the controllers and robustness analyses [8]. Thus, four individual control loops can be considered, namely: BRG, for the Bragg angle; and GAP, PTC and RLL, for the inter-crystals gap, and the pitch and roll angles, in the so-called crystal cage (CCG), respectively.

Feedback The first step consists in designing robust feedback controllers, which is done via the loop-shaping technique [9]. Indeed, thanks to the damped mass-spring approximation (second-order system) with low-frequency decoupling that characterizes the plants of the four loops (see [8]), simple and generic proportional-integral-derivative (PID) controllers can be implemented with practical "rules of thumb" [10].

First, the bandwidth frequencies, defined as those in which the open-loop transfer functions cross 0 dB, are chosen as $f_{bw} = 20$ Hz for the BRG and $f_{bw} = 250$ Hz for the CCG loops. Then, for phase margin, a lead filter is added with a zero at $f_{bw}/3$ and a pole at $3f_{bw}$. Next, to avoid high-frequency amplification of dynamics and reduce sensor noise, a low-pass filter is added at $5f_{bw}$. After that, an integral action is added with a zero at $f_{bw}/5$ for zero-frequency (DC) error. Finally, analyzing the open-loop system for gain and phase margins, a couple of notch filters may be added as necessary. Here, 2 notches are used for the RLL loop and 1 for the remaining ones. The modeled feedback closed-loop

ISBN: 978-3-95450-221-9 ISSN: 2226-0358 doi:10.18429/JACoW-ICALEPCS2021-WEPV003

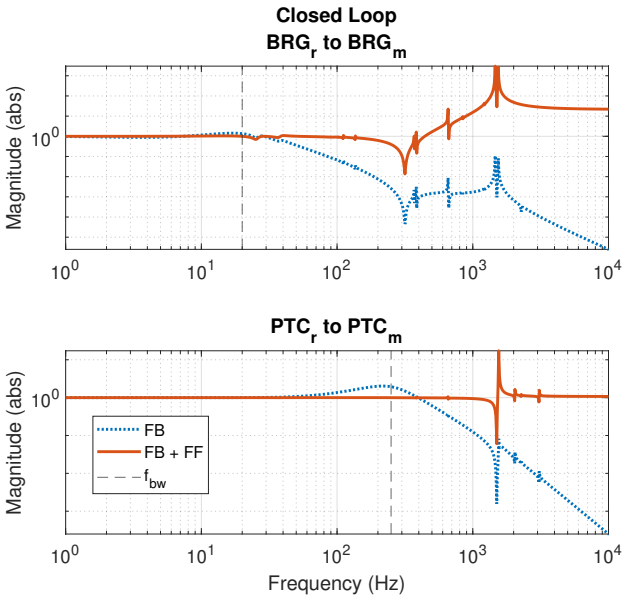

Figure 2: BRG and PTC transfer functions for the feedback closed-loop and for a feedback plus feedforward equivalent. The feedback bandwidths are also indicated in dashed lines.

transfer functions from reference (r) to output (m) for BRG and PTC can be seen in Fig. 2.

Feedforward To reduce the transient errors and expand the demanding scanning possibilities beyond the feedback bandwidth limits, particularly for the BRG loop, simple feedforward filters are also included in the model. Thus, assuming well-designed trajectory setpoints, with limited energy content in the high-frequency range, and once again benefiting from the reasonable second-order approximation for the plants in the low and mid-frequency ranges, high-order inversion-based filters can be prevented, and the feedforward blocks can be simply based on stiffness, damping and inertia constants.

In the model, the parameters can be directly extracted and perfectly compensated for. In practice, experimental tuning shall be realized. In this sense, this simplified feedforward structure will also ease the experimental tuning, thanks to the small number of parameters, in addition to saving implementation resources in the control hardware.

As an indication of the intended concept, the simulated transfer functions from reference (r) to output (m) with feedback plus feedforward for BRG and PTC are also depicted in Fig. 2. It can be seen that setpoints over a broader frequency range should be possible thanks to the feedforward action, but also that the energy content of these setpoints (visible in Fourier analyses, for instance) should be carefully designed below 200 Hz to prevent issues, such amplification effects and saturation, especially in the BRG loop.

DISTURBANCE MODELS

Once the mechatronic model has been built, the disturbances that will eventually determine the system performance must be addressed. Conceptually, they may be grouped as mechanical disturbances, as forces acting on the system, and electronic disturbances, which are related to the control hardware.

The main mechanical disturbances are the floor vibrations (GND) and Flow-Induced Vibrations (FIV) induced by the cryogenic cooling architecture of the silicon crystals via liquid nitrogen (see [11]). For the GND, the floor spectra is directly available from measurements with accelerometers and seismoemeters. Modeling FIV disturbances, on the other hand, is far more challenging due to the complexity of the flow effects and the cryogenic conditions required for real measurements. Thus, FIV was modeled according to best guesstimates. Theses disturbances are described in details for the HD-DCM in [3] and reused here.

The electronic disturbances, in turn, can be subdivided into actuators and sensors. All actuators will be controlled via the NI-9269 digital-to-analog converter (DAC), with a certain contribution in electronic noise, such as quantization. Then, the Aerotech APR260-S-240-83 rotary stages will use the Varedan LA-415-SA-T linear amplifier, whereas the Akribis AVM40-HF-6.5 voice-coils will rely on Trust Automation TA105. Each amplifier has its own noise level and spectral signature, affecting the closed-loop control error. Regarding the sensors, the rotary stages will be based on Renishaw TONIC encoders, whereas the sensors in the CCG will be SmarAct PicoScale Michelson interferometers. This electronic noise also enters the closed-loop system as disturbances. All these elements were already experimentally characterized for HD-DCM, as detailed in [3] as well.

SDE

While, as demonstrated in [3], the previous disturbance sources are sufficient to predict and describe the HD-DCM and the HD-DCM-Lite performances in stand-still condition, another type of sensor disturbance is introduced during motion, which becomes critical for the fast scanning purposes of the HD-DCM-Lite. Indeed, Sub-divisional Errors (SDE) are periodical patterns that are commonly found in optical sensors, such as encoders and interferometers, resulting from the measurement physical principles, together with alignment characteristics, and each particular electronic processing [12].

Based on empirical data, the SDE of the interferometers were found to be in the order of ± 2 nm with a periodicity of 775 nm (i.e. half of its infrared wavelength), which has a negligible impact on the control error of the system. The SDE for rotary encoder, on the other hand, reaches 300 nrad of amplitude with a periodicity of 10 µm (i.e. half of the scale pitch), which translates to about 100 µrad given the scale size. Since the typical stand-still control errors in the rotary stages are in the range of few tens of nrad RMS (see Table 1 in the Performance Predictions section), the harmful potential of the encoder SDE becomes clear.

Being artifacts, these patterns are deviations from the ideal measurements, and intrinsic accuracy limitations in the sensors, which can not be differentiated by the control

ISBN: 978-3-95450-221-9 ISSN: 2226-0358 doi:10.18429/JACoW-ICALEPCS2021-WEPV003

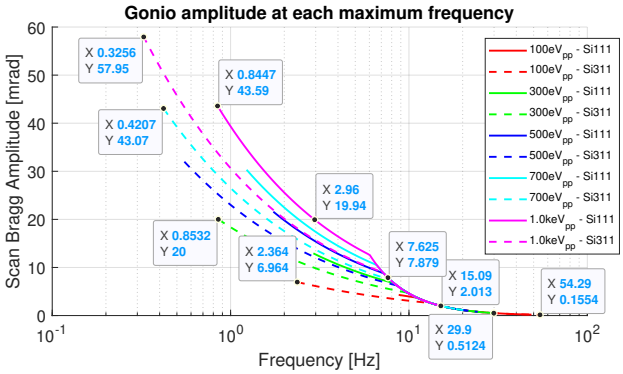

Figure 3: Boundary scanning possibilities for different energy scan amplitudes with either crystal set and ten representative points for performance analysis.

loop *a priori* from what would be the ideal signal. Thus, during motion, unless more advanced calibration and filtering strategies can be implemented via control, these errors appear at frequencies related to the traveling speed, being introduced in the closed control loop through its complementary sensitivity function.

Hence, at low frequencies the errors are followed by the system, around the bandwidth frequency they are amplified, and then they are gradually filtered out for increasingly higher frequencies. In the following and amplification regions these errors are converted to actuation effort (torque), which may excite internal mechanical resonances or at least increase the disturbances to the CCG control loops. This is why this effect must be carefully investigated.

Still, as the encoder SDE contribution depends completely on the trajectory being executed, some assumptions must be made for modeling purposes. Considering that as many repetitive energy scans per second as possible are desired for spectroscopy experiments with the HD-DCM-Lite, torque and motion disturbances can be expected to be minimized for sinusoidal trajectories in the rotary stage.

Taking into account all practical boundary limitations, and the non-linear relations among the desired energy and the Bragg angle for both crystal sets and gap between crystals, Fig. 3 provides an abacus with maximum expected scanning frequency for the Bragg amplitudes related to different energy scan amplitudes (see [5]). Finally, given the sinusoidal trajectories, the SDE can be modeled via *sine sweeps*, in which the maximum frequency is proportional to the maximum sinusoidal angular speed. Ten case studies selected for performance analysis in the following section are also highlighted in Fig. 3.

PERFORMANCE PREDICTIONS

Having the mechatronic and disturbance models, the performance predictions can be finally derived in the DEB toolbox. Thanks to the superposition nature of the linear time-invariant (LTI) formalism, the role of the different error sources can be independently investigated, which, in particular, allows for straightforward comparisons between static and scanning performances. Since the low frequency content of the reference trajectories should be mostly handled by feedforward, the SDE becomes the main additional noise source during scans.

A graphical example of one such performance prediction is illustrated in the cumulative power spectrum (CPS) plots in Fig 4, with the disturbances grouped according to what was presented in the Disturbances section. It shows the leftmost case of Fig. 3, i.e. sinusoidal scans with the largest Bragg amplitude (around 60 mrad, or 3.4 deg) and lowest sinusoidal scanning frequency (around 0.3 Hz). It can be seen that the SDE has a brutal effect in the BRG loop, being more than 10 times larger than the second highest effect, which is the GND. The total error approaches 0.5 µrad, which exceeds the original spec of 0.15 µrad by more than a factor 3, requiring some attention, as discussed below.

Similarly, for the PTC, which is the most sensitive control loop for beam position variation, the SDE dominates the error budget, with the 10 nrad spec being marginally exceeded. Without it, representing the stand-still condition, the errors are limited to about 5 nrad only. For the GAP and RLL loops, in turn, most of the contribution is due to the floor vibrations, with negligible contributions from the remaining elements. Still the values are well within the specs of 300 nm and 90 nrad, respectively.

The complete prediction results, with the RMS (1 Hz-2.5 kHz) control error for all simulated sinusoidal scan trajectories, are summarized in Table 1. The stand-still subset and original specification are also indicated in the last rows for completeness. It should be noted that the frequency and angular amplitude are identifying the scans according to Fig. 3, but these two parameters alone are not sufficient to fully describe a scan, since the mean energy also plays a role. Nonetheless, it is possible to notice that the SDE influence grows with the scanning frequency, as it might be expected.

It can be seen the the BRG loop is the one that is most critically affected by the SDE, with the errors exceeding the original spec by more than a factor 10. Still, the PTC also shows increasing errors with higher scanning frequencies, reaching nearly 40 nrad. Thus, a future topic of research is looking for a practical solution for filtering the sweeping SDE contribution via control or calibration. In the meantime, if truly sensitive to these error levels, the experiments may need to be limited to sufficiently lower scanning frequencies.

Furthermore, it is worth mentioning that, while the CCG loops are practically implemented as followers of the BRG loop, due to the geometrical relation of the gap and to fine calibrations with respect to the Bragg angle (see [13]), the appropriate leading signal must come from the BRG reference, not its sensor (see also [6]). All the performance results presented here follow this approach. Indeed, the control errors in the BRG are small as far as the gap and the calibration parameters are concerned, such that the reference signal provides a sufficiently accurate reference for the remaining loops. Otherwise, if following the measurement signal, the whole dynamics of the BRG loop, including its

ISBN: 978-3-95450-221-9 ISSN: 2226-0358 doi:10.18429/JACoW-ICALEPCS2021-WEPV003

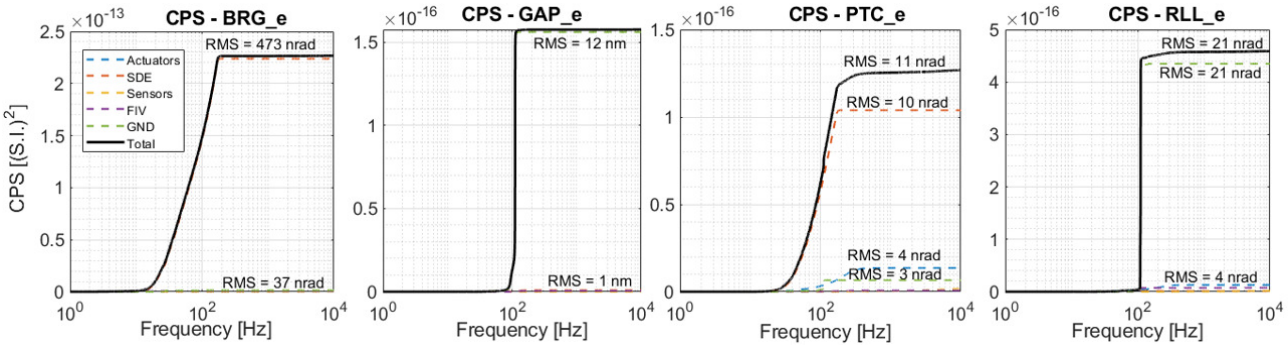

Figure 4: Cumulative power spectrum (CPS) according to the DEB simulations considering all the disturbance sources for a sinusoidal scan with $f = 0.3$ Hz and $\theta_A = 60$ mrad.

Table 1: Position stability (RMS) results for disturbances on control loops for different scan amplitudes θ_A and frequencies f between 1 kHz to 2.5 kHz

θ_A [mrad]	f [Hz]	BRG_e [nrad]	GAP_e [nm]	PTC_e [nrad]	RLL_e [nrad]
60	0.3	470	12	11	21
40	0.4	450	12	11	21
40	0.9	430	12	9.6	21
20	0.9	460	12	11	21
20	3.0	780	12	13	21
7.0	2.4	1000	12	22	21
8.0	7.7	1600	12	24	22
2.0	15	1800	13	36	22
0.5	30	1300	13	30	22
0.2	54	1600	13	38	22
No SDE:		55	12	4.8	21
Spec:		150	300	10	90

SDE errors would couple to the CCG loops, more significantly degrading their performances.

The scanning results discussed here find their most direct potential at bending magnet beamlines, such as QUATI, due to their broad-band emission spectra. With undulators, opportunities will depend on motion limitations, including the potential influences on the storage ring, and detuned operation possibilities. Hence, in the short term, integration and synchronization efforts are expected to be focused mainly between the monochromator and the detectors (which may reach acquisition rates of a few MHz). In that sense, promising initial results have been recently demonstrated with the HD-DCM (see [14] and [15]).

Finally, one potential disturbance source that may turn out to have a significantly negative impact in scans is the mechanical bearings in the rotary stage. The reason why it has been left out of the analyses, was the difficulty in modeling it, given the strong non-linear dependencies on mechanical tolerances, payload, speed and lubrication/friction. Consequently, although conservative in the modeled disturbances, the numbers presented here cannot be considered fully conservative performance predictions for the HD-DCM-Lite design. The commissioning results with the first prototype, due to the next few months, will provide further insights and occasionally suggest that smoother bearings, such as contactless air bearings or magnetically levitating bearings, may be required for ultimate performance.

CONCLUSION

Dynamic error budgeting (DEB) is a powerful methodology to be used in the predictive design of high-performance mechatronic systems. The toolbox developed in-house over the course of the High-Dynamic Double-Crystal Monochromator (HD-DCM) project is now applied in the development of the HD-DCM-Lite for extended scanning capabilities at Sirius light source. The model predictions, which provided very good agreement with experimental data in the HD-DCM, here point to an unprecedented inter-crystal parallelism level in the range of 5 nrad RMS (1 Hz – 2.5 kHz) in stand-still conditions. Yet, the results also suggest that the detrimental effects of sub-divisional errors (SDE) in the sensors to the most demanding scanning trajectories might increase the control errors by more than a factor 10. The actual impact of the occasional performance reduction may need to be confronted with particular experimental sensitivity at the beamlines, but effective filtering strategies should be investigated as soon as possible. Finally, possibly limiting disturbances arising from the mechanical bearings during scans will require deeper experimental investigations during commissioning, which is expected by early 2022.

ACKNOWLEDGEMENT

The authors would like to gratefully acknowledge the funding by the Brazilian Ministry of Science, Technology and Innovation and the contributions of the LNLS team. They also recognize the essential role of MI-Partners in the development of the original HD-DCM and in the workflow adopted here, and the discussions that allowed for the development of many of the tools used in this work as part of a PhD project carried out with the CST group at TUe, with Marteen Steinbuch and Hans Vermeulen as promoters, and Gert Witvoet as co-promoter.

ISBN: 978-3-95450-221-9 ISSN: 2226-0358 doi:10.18429/JACoW-ICALEPCS2021-WEPV003

REFERENCES

[1] R. Geraldes *et al.*, "The Status of the New High-Dynamic DCM for Sirius," en, *Proceedings of the Mechanical Eng.~Design of Synchrotron Radiation Equipment and Instrumentation*, vol. MEDSI2018, 6 pages, 1.106 MB, 2018, Artwork Size: 6 pages, 1.106 MB ISBN: 9783954502073 Medium: PDF Publisher: JACoW Publishing, Geneva, Switzerland. DOI: 10.18429/JACOW-MEDSI2018-WEOAMA01. http://jacow.org/medsi2018/doi/JACoW-MEDSI2018-WEOAMA01.html

[2] O. Müller, D. Lützenkirchen-Hecht, and R. Frahm, "Quick scanning monochromator for millisecond *in situ* and *in operando* X-ray absorption spectroscopy," en, *Review of Scientific Instruments*, vol. 86, no. 9, p. 093 905, Sep. 2015, ISSN: 0034-6748, 1089-7623. DOI: 10.1063/1.4929866. http://aip.scitation.org/doi/10.1063/1.4929866

[3] R. R. Geraldes, M. A. L. Moraes, R. M. Caliari, and G. Witvoet, "Dynamic Error Budgeting in the development of the High-Dynamic Double-Crystal Monochromator for Sirius light source," *American Society for Precision Engineering Topical Meetings*, 2020.

[4] L. Jabben and J. van Eijk, "Performance analysis and design of mechatronic systems," *Mikroniek - Professional Journal on Precision Engineering*, vol. 51, no. 2, pp. 5–11, 2011, bibtex[publisher=Dutch Society for Precision Engineering].

[5] A. V. Perna *et al.*, "The HD-DCM-Lite: A High-Dynamic DCM with Extended Scanning Capabilities for Sirius/LNLS Beamlines," in *presented at the 11th Mechanical Engineering Design of Synchrotron Radiation Equipment and Instrumentation Int. Conf. (MEDSI'20)*, JACoW Publishing, Jul. 2021.

[6] R. R. Geraldes *et al.*, "The fpga-based control architecture, epics interface and advanced operational modes of the high-dynamic double-crystal monochromator for sirius/lnls," in *presented at the 18th Int. Conf. on Accelerator and Large Experimental Physics Control Systems (ICALEPCS'21)*, (Shanghai, China), JACoW Publishing, Oct. 2021.

[7] D. de Klerk, D. J. Rixen, and S. N. Voormeeren, "General Framework for Dynamic Substructuring: History, Review and Classification of Techniques," en, *AIAA Journal*, vol. 46, no. 5, pp. 1169–1181, May 2008, ISSN: 0001-1452, 1533-385X. DOI: 10.2514/1.33274. https://arc.aiaa.org/doi/10.2514/1.33274

[8] R. M. Caliari, R. R. Geraldes, M. A. L. Moraes, and G. Witvoet, "Loop-Shaping Controller Design in the Development of the High-Dynamic Double-Crystal Monochromator at Sirius Light Source," *American Society for Precision Engineering Topical Meetings*, 2020.

[9] S. Skogestad and I. Postlethwaite, *Multivariable feedback control: analysis and design*, 2nd ed. Hoboken, NJ: John Wiley, 2005, ISBN: 978-0-470-01167-6.

[10] R. M. Schmidt, G. Schitter, and J. v. Eijk, *The design of high performance mechatronics: high-tech functionality by multidisciplinary system integration*, English. 2020, OCLC: 1145888837, ISBN: 978-1-64368-051-4. https://search.ebscohost.com/login.aspx?direct=true&scope=site&db=nlebk&db=nlabk&AN=2401172

[11] R. Geraldes *et al.*, "The New High Dynamics DCM for Sirius," en, *Proceedings of the 9th Edition of the Mechanical Engineering Design of Synchrotron Radiation Equipment and Instrumentation Conference*, vol. MEDSI2016, 6 pages, 0.966 MB, 2017, Artwork Size: 6 pages, 0.966 MB ISBN: 9783954501885 Medium: PDF Publisher: JACoW Publishing, Geneva, Switzerland. DOI: 10.18429/JACOW-MEDSI2016-TUCA05. http://jacow.org/medsi2016/doi/JACoW-MEDSI2016-TUCA05.html

[12] A. Ellin and G. Dolsak, "The design and application of rotary encoders," en, *Sensor Review*, vol. 28, no. 2, J. Billingsley, Ed., pp. 150–158, Mar. 2008, ISSN: 0260-2288. DOI: 10.1108/02602280810856723. https://www.emerald.com/insight/content/doi/10.1108/02602280810856723/full/html

[13] R. R. Geraldes *et al.*, "Commissioning and Prospects of the High-Dynamic DCMs at Sirius/LNLS," in *presented at the 11th Mechanical Engineering Design of Synchrotron Radiation Equipment and Instrumentation Int. Conf. (MEDSI'20)*, JACoW Publishing, Jul. 2021.

[14] R. R. Geraldes *et al.*, "Design and Commissioning of the TARUMÃ Station at the CARNAÚBA Beamline at Sirius/LNLS," in *presented at the 11th Mechanical Engineering Design of Synchrotron Radiation Equipment and Instrumentation Int. Conf. (MEDSI'20)*, JACoW Publishing, Jul. 2021.

[15] J. R. Piton *et al.*, "Tatu: A flexible fpga-based trigger and timer unit created on compactrio for the first sirius beamlines," in *presented at the 18th Int. Conf. on Accelerator and Large Experimental Physics Control Systems (ICALEPCS'21)*, (Shanghai, China), JACoW Publishing, Oct. 2021.